Vol. 592: 77–95, 2018
https://doi.org/10.3354/meps12481

MARINE ECOLOGY PROGRESS SERIES
Mar Ecol Prog Ser

Published March 29

# Production and consumption of extracellular polymeric substances in an intertidal diatom mat

**Tanja C. W. Moerdijk-Poortvliet[1,2,*], Olivier Beauchard[1,3,4], Lucas J. Stal[1,5], Henricus T. S. Boschker[1]**

[1]NIOZ Royal Institute for Sea Research and Utrecht University, PO Box 140, 4401 AC Yerseke, The Netherlands
[2]HZ University of Applied Sciences, Chemistry Department, PO Box 364, 4380 AJ Vlissingen, the Netherlands
[3]Flanders Marine Institute (VLIZ), InnovOcean site, Wandelaarkaai 7, 8400 Oostende, Belgium
[4]University of Antwerp, Department of Biology, Ecosystem Management Research Group (ECOBE), Universiteitsplein 1, 2610 Antwerpen, Belgium
[5]University of Amsterdam, Department of Freshwater and Marine Ecology, PO Box 94248, 1090 GE Amsterdam, The Netherlands

ABSTRACT: We investigated seasonal changes in the production of extracellular polymeric substances (EPS) and short-chain organic acids (SCOA) exuded by benthic diatoms, and the use of these exudates as a carbon source by heterotrophic bacteria. An *in situ* $^{13}C$ pulse-chase method was used to follow the fate of EPS for 5 consecutive days. These experiments were done at 2 mo intervals for 1 yr. The EPS were recovered from the sediment as 2 operationally defined fractions (i.e. water-extractable and EDTA-extractable EPS). Seasonal differences in EPS production correlated to light intensity and temperature. From February until June the biomass and production of diatoms and bacteria were closely coupled. It was concluded that SCOA were the most important substrates for the bacteria. Sulfate-reducing bacteria (SRB) in particular benefited from SCOA released by diatoms. From August on, the coupling of biomass and production of diatoms and bacteria weakened and was almost lost in December. During the period from August to December, EPS produced by diatoms promoted the growth of other bacterial taxa rather than SRB, and the production of SCOA was low. Thus, it appears that the seasonal variation in exudates produced by diatoms plays an important role in shaping community composition and maintaining the diversity of the associated bacteria.

KEY WORDS: Microphytobenthos · *In situ* $^{13}C$-labeling · Extracellular polymeric substances



## INTRODUCTION

Intertidal sediments support extensive and diverse populations of microorganisms, which develop into complex microbial communities. In temperate regions, benthic diatoms are the dominant organisms of the microphytobenthic communities; the biofilms they produce color the sediment surface brown. The diatoms contribute a major part of the total autotrophic production in these intertidal benthic ecosystems (Admiraal et al. 1984, MacIntyre & Cullen 1996, Underwood & Kromkamp 1999). These benthic diatom mats exhibit high rates of photosynthesis, and a substantial proportion of the inorganic carbon they fix may be exuded into the environment as extracellular polymeric substances (EPS) or short-chain organic acids (SCOA) (Underwood & Paterson 2003, Miyatake et al. 2014). In addition to direct release by diatoms, SCOA may also be produced as fermentation products during the anaerobic degradation of diatom EPS (McKew et al. 2013). EPS- and SCOA-releasing diatoms stimulate bacterial growth, and the great variety of substrates

*Corresponding author: tanja.moerdijk@gmail.com

could play a role in generating and maintaining bacterial diversity (Amin et al. 2012).

EPS are exuded through various mechanisms and play an important role in the ecology of diatom mats (Edgar & Pickett-Heaps 1984). For instance, EPS exudation allows motility of diatoms, which is crucial for epipelic species because it enables them to migrate into the sediment when the tide comes in, preventing them from being grazed, as well as providing them access to nutrients (Consalvey et al. 2004). Furthermore, EPS are sometimes produced as the result of unbalanced growth, i.e. growth that does not lead to proportional synthesis of the cell's structural components because essential nutrients (e.g. nitrogen, phosphorus, sulfur and iron) are lacking or limiting, and components are synthesized that lack these nutrients (e.g. carbohydrates and lipids) (Stal 2010). Because the cell's storage capacity is limited, excess fixed carbon is exuded as EPS. After exudation, EPS accumulate in the surficial sediments where they become available for heterotrophic bacteria, or are washed away during tidal immersion and/or become part of the biofilm matrix (Yallop et al. 1994, Stal 2010, Taylor et al. 2013). EPS comprise either low-molecular-weight dissolved compounds or consist of more complex colloidal or gel-like material, such as mucilage. The diatoms, the mucilage, and the sediment produce a coherent structure — the biofilm or mat — that stabilizes the sediment surface and avoids re-suspension of the diatoms. EPS may further serve to protect the diatoms from environmental stress due to changes in temperature, salinity, nutrient availability, desiccation, and UV radiation (Hoagland et al. 1993, Underwood & Paterson 2003). Last but not least, EPS provide a carbon source to the benthic food web, which includes heterotrophic bacteria (Middelburg et al. 2000).

EPS formation by benthic diatoms has been extensively studied. However, thus far most studies have been done in pure cultures and/or focused on the measurement of the content of EPS fractions, thereby neglecting effects of community interactions, production, and turnover rates of these exudates (Smith & Underwood 1998, Pierre et al. 2014). Most research has been carried out on the dominant carbohydrate component of these exudates, which is undoubtedly important in sediment carbon cycling (Bellinger et al. 2009, Oakes et al. 2010, Taylor et al. 2013). However, EPS may also contain proteins, lipids, nucleic acids, and other biopolymers such as humic substances (Flemming & Wingender 2010). Carbohydrates are known to be major intermediates in the rapid transfer of carbon between diatoms and heterotrophic bacteria (Middelburg et al. 2000, Evrard et al. 2008, Bellinger et al. 2009, Taylor et al. 2013). Besides gaining knowledge on EPS dynamics, understanding interactions between diatoms and heterotrophic bacteria is important as they modify each other's behavior and eventually impact biogeochemical cycles (Bruckner et al. 2011, Amin et al. 2012).

The research question of this exploratory study was how carbon, which originated from EPS and SCOA produced by diatoms, flows to the heterotrophic bacterial community in an intertidal mudflat and how this flow changes seasonally. By using an *in situ* $^{13}C$ pulse-chase method (Middelburg et al. 2000) in combination with liquid chromatography isotope ratio mass spectrometry (LC/IRMS), it was possible to follow the fate of the applied $^{13}C$ label from carbon fixation to EPS and SCOA exudation (Moerdijk-Poortvliet et al. 2014, 2018). Here, using the same experiment as Moerdijk-Poortvliet et al. (2018), we followed the fate of the applied $^{13}C$ label to the heterotrophic bacteria. Phospholipid-derived fatty acid (PLFA) biomarker analysis was used to differentiate between benthic diatoms and different groups of heterotrophic bacteria.

## MATERIALS AND METHODS

### Study site and *in situ* $^{13}C$-labeling experiments

In 2011, *in situ* $^{13}C$-labeling experiments were carried out at approximately 2 mo intervals at the Zandkreek intertidal mudflat, situated along the southern shore of the Oosterschelde estuary in the southwest of the Netherlands (51° 32′ 41″ N, 3° 53′ 22″ E). The sampling site was located 0.15 m below the mean tidal level, and the emersion period was approximately 6 h per tidal cycle. Bioturbating fauna such as the amphipod crustacean *Corophium volutator* and the hydrobiid snail *Peringia ulvae* became active starting late spring (June), gaining higher grazing rates and mixing the sediment top layer during summer. Detailed information on the study site and sampling is found in Moerdijk-Poortvliet et al. (2018).

Experiments started immediately after emersion of the mudflat. Two 500 × 500 mm stainless steel frames were pushed into the sediment to a depth of 80 mm in order to constrain the labeling and sampling area. The 2 frames were treated as duplicates (n = 2) and were divided in a 100 × 100 mm sampling grid. Unlabeled control samples were taken just outside the frames as described below. The *in situ* labeling experiment started by spraying the surface of the sedi-

ment within each frame with 200 ml of [$^{13}$C] sodium bicarbonate (99% $^{13}$C; Cambridge Isotope Laboratories) with ambient salinity (30‰) to obtain a final concentration of 1 g $^{13}$C m$^{-2}$ (Middelburg et al. 2000).

The labeled sediment was sampled 2 and 4 h after label addition during the first low tide (the pulse-labeling period), and subsequently at 12 h, 1 d, 2 d, 3 d, and 5 d exactly at low tide (the chase period). At each sampling time, pore water was collected from 2 randomly chosen positions within the sampling grid of each stainless steel frame using porous polymer sippers (Rhizon Soil Moisture Sampler; Eijkelkamp Agrisearch Equipment) inserted into the upper 15 mm of the sediment, and these 2 samples were combined (total ~5 ml). For each stainless steel frame, 1 ml of pore water was injected into airtight headspace vials and analyzed for $^{13}$C-dissolved inorganic carbon (DIC); the remainder was used for inorganic nutrient analysis and SCOA analysis. Water column nutrient data were obtained from the Netherlands Institute for Sea Research (NIOZ) monitoring program from a station 500 m away from the experimental site.

Sediment samples were collected and mixed from 2 randomly chosen positions within the sampling grid of each steel frame. The top 15 mm of the sediment was collected by pushing a core liner (inside diameter 100 mm) into the sediment to a depth of 50 mm, and subsequently the top 15 mm of the sediment was sampled with a spatula (Middelburg et al. 2000). The corer was removed and the sampling hole was filled with unlabeled sediment collected just outside the experimental area. The 2 sediment samples taken from each steel frame area were homogenized and subsampled for the various analyses. Samples for PLFA analysis were directly frozen in liquid nitrogen and subsequently lyophilized and stored at −20°C until analysis. Samples for pigment analysis were also directly frozen in liquid nitrogen and were subsequently stored at −80°C prior to analysis. Sediment samples for EPS extraction were transported to the laboratory within 30 min after sampling and subsequently processed as described in Miyatake et al. (2014). For all experiments, 2 operationally defined EPS were extracted: water-extractable EPS (EPS MQ) using freshly prepared Milli-Q water (MQ, 18.2 MΩ, DOC free; Millipore) and EDTA-extractable EPS (EPS EDTA). To ~4 g wet weight of the homogenized sample, 4.5 ml Milli-Q water was added for EPS MQ extraction as described in de Brouwer & Stal (2001). Samples were shaken for 1 h at 30°C in the dark and centrifuged at 4000 × *g* for 15 min. The supernatant was stored at −20°C, and the pellet was re-extracted with 4.5 ml of 0.1 M EDTA by shaking for 4 h in the dark at room temperature. The supernatant was collected after centrifugation at 4000 × *g* for 15 min and stored at −20°C. Both extracts were analyzed for carbohydrates (CHO) and amino acids (AA). In total, 4 operationally defined EPS fractions were distinguished: CHO MQ, CHO EDTA, AA MQ and AA EDTA.

In order to study dark fixation by chemoautotrophic and heterotrophic bacteria, 2 cores (70 mm inner diameter) were taken outside the experimental area and incubated in the dark for 4 h with the same amount of $^{13}$C-label (per m$^2$) as used in the experimental area added to the top of the sediment. The top 15 mm of the core was sampled and analyzed for PLFA labeling.

Miniaturized pulse amplitude modulated (PAM) fluorometry (Mini-PAM; Walz) was used to measure photosynthetic parameters. Intact sediment cores of the diatom mat were taken in duplicate. Rapid light curves (RLCs) were recorded simultaneously with the pulse-labeling period. Prior to recording RLCs, samples were dark-adapted for 15 min to relax photochemical quenching. Subsequently, RLCs were recorded with 12 incremental irradiance steps of 20 s. From these data, the relative maximum photosynthetic electron transport, the light affinity coefficient (α), and the light saturation irradiance were determined (Serôdio et al. 2005).

During the $^{13}$C label incorporation and RLC recordings, PAR (400 to 700 nm) was measured on-site every 15 min by a LICOR light meter (LI-250A) connected to a quantum sensor (LI-190R; Li-cor). Throughout the year, a PAR sensor (LI 191; Licor) connected to a data logger (LI-1000; Licor), located 10 km from the study area, measured PAR values every 1 min; these data were averaged and logged hourly. The light sensors were cosine-corrected.

### Analytical procedures

For DIC analysis, pore water samples were acidified by adding 0.1 ml of 19 M phosphoric acid (Miyajima et al. 1995), and headspace gas was analyzed by elemental analyzer/isotope ratio mass spectrometry (EA/IRMS) in order to determine the concentration and isotopic composition of DIC.

Carbon content and isotopic composition of EPS and SCOA were analyzed by LC/IRMS. For carbohydrates, 4 ml EPS extract was hydrolyzed under acidic conditions to monosaccharides using a modified method according to Cowie & Hedges (1984). The method was modified by neutralizing the hydrolyzed samples with strontium carbonate instead of barium

carbonate, which resulted in an increased yield of the extract. For the EPS EDTA extracts, the EDTA was removed from the hydrolyzed samples as described in Moerdijk-Poortvliet et al. (2014). Carbohydrates were analyzed by LC/IRMS as described in Boschker et al. (2008). For amino acids, 4 ml EPS extract was hydrolyzed with 6 M HCl for 20 h at 110°C and subsequently purified by cation exchange chromatography (Veuger et al. 2005) and analyzed by LC/IRMS as described in McCullagh et al. (2006). SCOA were examined without additional sample preparation and analyzed by LC/IRMS equipped with an Aminex HPX-87H cation exchange column (Bio-Rad Laboratories). The eluent was 8 mM sulfuric acid at a flow rate of 0.4 ml $min^{-1}$ (Krumböck & Conrad 1991). Liquid chromatography was carried out using a Surveyor liquid chromatograph connected to an LC Isolink interface and a Delta V Advantage IRMS (all from Thermo Fisher Scientific).

Lipids were extracted from 4 g dry weight of sediment with a modified Bligh and Dyer extraction (Boschker et al. 1999). The lipid extract was fractionated on silicic acid (60; Merck) into different polarity classes by sequential eluting with chloroform, acetone, and methanol. The chloroform fraction contained mainly neutral lipid-derived fatty acids, while the acetone and methanol fraction contained polar lipid-derived fatty acids (i.e. mainly glycolipid-derived fatty acids and PLFAs, respectively, but both fractions also contained other lipids such as betaine lipids and sulfolipids) (Heinzelmann et al. 2014). The methanol fraction was denoted as the PLFA fraction and converted into fatty-acid methyl esters, and the carbon content and isotopic composition of these derivatives were measured by gas chromatography isotope ratio mass spectrometry (Middelburg et al. 2000, Boschker 2004).

Pigments were extracted with acetone (90%, buffered with 5% ammonium acetate) from freeze-dried sediment and analyzed by reverse-phase high-performance liquid chromatography (Dijkman & Kromkamp 2006).

Nutrients were measured using a segmented continuous flow analyzer (SEAL QuAAtro XY-2 autoanalyzer, Bran and Luebbe) according to the instructions provided by the manufacturer.

### Data analysis

The absolute amount of $^{13}C$ incorporated into EPS fractions, SCOA, and PLFA in excess of the background was displayed. This value is expressed as excess $^{13}C$ (in mol $^{13}C$ $m^{-2}$) and is calculated from $\delta^{13}C$ sample as:

$$\text{Excess } {}^{13}\text{C} = \left\{ \left[ \frac{\left(\delta^{13}C_{sample}/1000+1\right)\times R_{standard}}{\left(\delta^{13}C_{sample}/1000+1\right)\times R_{standard}+1} \right] - \left[ \frac{\left(\delta^{13}C_{background}/1000+1\right)\times R_{standard}}{\left(\delta^{13}C_{background}/1000+1\right)\times R_{standard}+1} \right] \right\} \times C_{sample} \quad (1)$$

where $\delta^{13}C_{background}$ denotes the $\delta^{13}C$ value of the unlabeled sample and $C_{sample}$ denotes the pool size in mol of carbon per square meter sediment (mol C $m^{-2}$). Production rates of various EPS fractions and PLFA biomarkers were quantified by calculating the regression slope from sample data (at 0, 2, and 4 h) (expressed in µmol $^{13}C$ $m^{-2}$ $h^{-1}$).

Excess $^{13}C$ in bacterial biomass was estimated from the label incorporated in bacterial-biomarker PLFA as excess $^{13}C$-bacterial biomass (mol $^{13}C$ $m^{-2}$) = Σ excess $^{13}C$ $PLFA_{bact}$ / (0.056 × 0.23), where $^{13}C$ $PLFA_{bact}$ is $^{13}C$ in bacterial-biomarker PLFA (i.e. i14:0, i15:0, ai15:0, i17:0, 17:1ω6c, cy-19:0, i17:1ω7c, 10Me16:0, and i17:1ω5c), 0.056 represents the average (±SD) PLFA content in bacteria in terms of carbon, and 0.23 ± 0.06 is the average fraction of these bacterial PLFA among total PLFA in bacteria-dominated marine sediments (Middelburg et al. 2000). Excess $^{13}C$ into diatom biomass was calculated from the difference between excess $^{13}C$ into all PLFA and excess $^{13}C$ into bacterial PLFA and was also corrected for the typical PLFA content of diatoms: excess $^{13}C$-diatom biomass (mol$^{13}C$ $m^{-2}$) = (Σ excess $^{13}C$ $PLFA_{all}$ – Σ excess$^{13}C$ $PLFA_{bact}$) / 0.035, where $^{13}C$ $PLFA_{all}$ is $^{13}C$ in all individual PLFA measured and 0.035 represents the average PLFA content of diatoms (Middelburg et al. 2000). Diatom and bacterial biomass were calculated as above in terms of carbon $m^{-2}$ sediment using the PLFA concentrations instead of excess $^{13}C$ values.

The relative photosynthetic electron transport rate (rETR) was calculated by multiplying the Mini-PAM-measured quantum yield (i.e. 'efficiency' of photosynthesis) and the applied irradiance ($E$) during the recording of the RLCs (Kromkamp & Forster 2003). From the RLCs, the relative maximum photosynthetic electron transport rate ($ETR_{max}$), the light affinity coefficient in the light-limited region of the rapid light curve (α), and the light saturating irradiance ($E_k = ETR_{max}/\alpha$) were determined by fitting the RLCs to a modified version of the equation of Eilers & Peeters (1988): $rETR = E/(aE^2 + bE + c)$, where $a = (\alpha \times E_k^2)^{-1} - 2 \times (\alpha \times E_k)^{-1}$; $c = \alpha^{-1}$.

Multivariate statistics were applied in order to identify the relationships between environmental, photosynthetic, and pigment parameters (i.e. expla-

natory variables; see Table A1 in the Appendix and Table S1 in the Supplement at www.int-res.com/articles/suppl/m592p077_supp.xlsx) and production rates of the EPS fractions (Table S2). The various EPS fractions might have originated from different processes and were correlated to the explanatory variables in such a way that the variables of the EPS fractions were kept in separate tables (samples × variables). The relationships between the explanatory variables and the different EPS fractions were explored by concordance analysis (Lafosse & Hanafi 1997). This approach is an extension of co-inertia analysis (Dolédec & Chessel 1994) that matches one table to several others. The inherent logic of co-inertia enables us to proceed with a large number of variables (Dray et al. 2003). Concordance analysis searches combinations of variables in each EPS fraction that co-vary and vary with combinations of explanatory variables. The number of variables does not affect the strength of the correlation because the tables are weighted by the inverse of their respective inertia. Because the EPS fraction data were percentages, they were log transformed and centered in column as recommended for compositional data (Aitchison 1983). Explanatory variables were log transformed and normalized. Prior to concordance analysis, the correlation between the explanatory variables and each EPS fraction was assessed by the RV-coefficient (Robert & Escoufier 1976). The significance was tested by a randomization procedure of 9999 permutations of table lines (Heo & Gabriel 1998). Hence, only the part of EPS significantly correlated to explanatory variables was considered in the concordance analysis. In the case of a single significantly correlated EPS table, the concordance analysis was a simple co-inertia analysis. Concordance analyses were run with ADE-4 software (Thioulouse et al. 1997), and associated graphical representations were made with the 'ade4' package (Chessel et al. 2004) in R version 3.2.3 (R Core Team 2015).

## RESULTS

### Seasonal dynamics of exudation and heterotrophic consumption of EPS and SCOA

An overview of the $^{13}C$ label in the carbon exuded by benthic diatoms, i.e. EPS and SCOA, is depicted in Fig. 1. In the 2 operationally defined EPS extracts (i.e. EPS MQ and EPS EDTA), we measured CHO as well as AA and, hence, we assigned 4 EPS fractions (CHO MQ, CHO EDTA, AA MQ, and AA EDTA). The $^{13}C$ labeling of bacteria (through the analysis of PLFA biomarkers) originated from the heterotrophic consumption of the extracellular carbon compounds released by the diatoms.

Most of the $^{13}C$ label was recovered in CHO MQ, followed by CHO EDTA, AA MQ, AA EDTA, and SCOA. The highest amount of $^{13}C$ label in all of these pools was observed in February and April (Fig. 1). Especially in February and April, an initial, steep increase of $^{13}C$ label was observed in the exuded carbon pools, followed by a steep decrease. During the rest of the year (June to December), EPS and SCOA were exuded and consumed at lower rates. The amount of $^{13}C$ label incorporated into the EPS and SCOA was highest between 4 and 12 h after the application of the label and subsequently disappeared during the course of the experiment (Fig. 1). The data suggest that the initial release of exudates was followed by a second (between 24 and 48 h) and sometimes even a third release (between 48 and 72 h). Labeling of the bacterial PLFA increased sharply during the first 4 h of the experiment and fluctuated over the course of the experiment. The increase of $^{13}C$ label in bacterial biomarkers coincided with the release of EPS and SCOA.

### Exudation and fate of EPS and SCOA carbohydrates and amino acids

Throughout the year, carbohydrates formed the main component of the extracellular fractions (68 to 91%) while amino acids represented a smaller proportion (9 to 32%) (Fig. 2a). Carbohydrates also explained most of the production of EPS (80 to 95%) (Fig. 2b). EPS production was strongly seasonal, while the EPS content of the sediment was less strongly affected by season.

Fig. 3 depicts the content of carbohydrates and amino acids of the EPS MQ and EPS EDTA extracts 4 h after the application of $^{13}C$ label (Fig. 3a–d) and after 3 d (Fig. 3e–h). This time was chosen because from Day 3 onwards the $^{13}C$ label distribution remained more or less the same. For carbohydrates as well as for amino acids, the relative $^{13}C$ label distribution in the monomers of the extracted EPS was different. For the CHO MQ fraction, most of the $^{13}C$ label was incorporated into glucose (80 ± 11%) (Fig. 3a) while in the CHO EDTA, the $^{13}C$ label was more evenly distributed between the monomeric carbohydrates (Fig. 3b). Most of the $^{13}C$ label in the AA MQ fraction was incorporated into proline (54 ± 11%) (Fig. 3c), while in the AA EDTA the highest

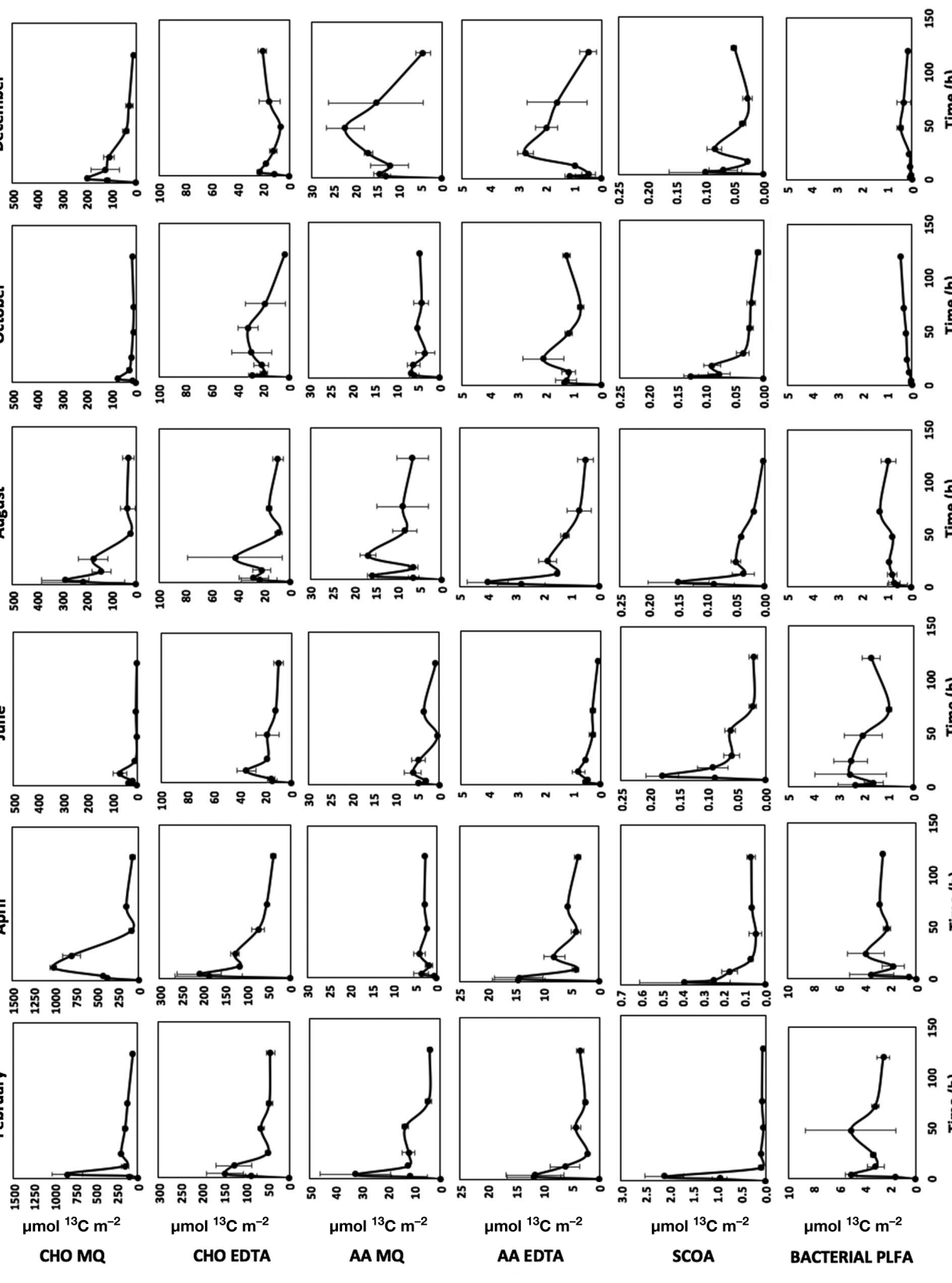


Fig. 1. Overview of $^{13}C$ label dynamics of excreted carbon pools (i.e. extracellular polymeric substances [EPS] and short-chain organic acids [SCOA]) and bacteria derived from heterotrophic consumption of these excreted carbon pools. In the 2 operationally defined EPS extracts (i.e. EPS MQ and EPS EDTA), carbohydrates and amino acids were detectable. Note that the *y*-axes of the panels for February and April differ from those of the other months (which are all the same). Also, the *y*-axes of the panels for SCOA for February and April are not identical. PLFA: phospholipid-derived fatty acids. Error bars are ± SD. See Table A1 in the Appendixfor other abbreviations

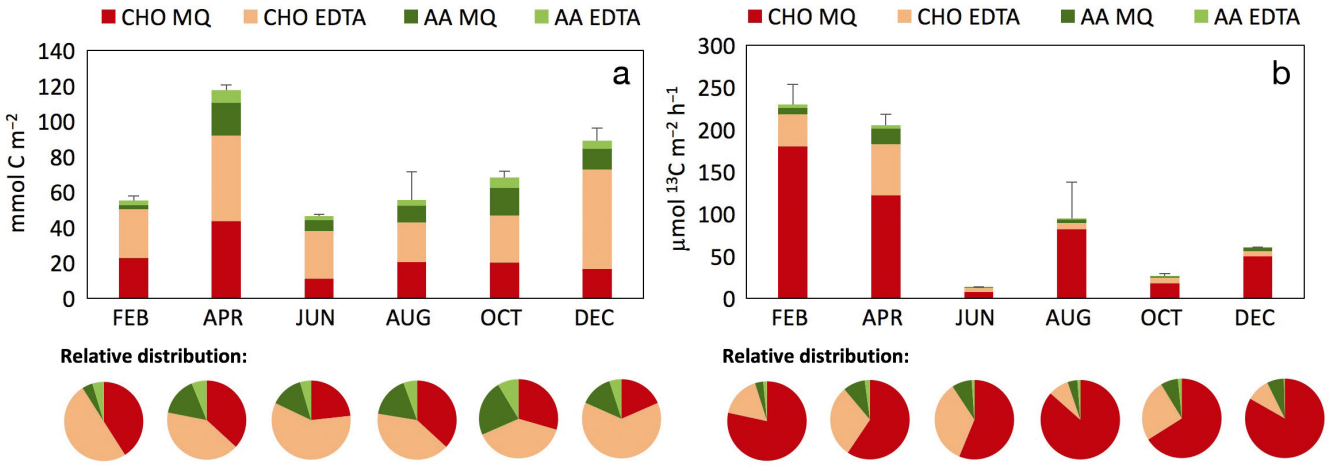


Fig. 2. Annual carbohydrate and amino acid (a) concentrations and (b) productions originated from water-extractable extracellular polymeric substances (EPS MQ) and EDTA-extractable EPS (EPS EDTA). Error bars are ± SD. See Table 2 for further abbreviations

amounts of $^{13}$C label were found in threonine, serine, and valine and depended on the season (Fig. 3d). Due to the elution of an unknown compound in the chromatogram of the AA EDTA fraction (which was substantial and comprised a large part of the chromatogram), the amino acids glycine, proline, and alanine could not be determined. Despite this limitation, it was ascertained that the AA EDTA fraction contained aspartate, serine, threonine, and methionine, which were not retrieved in the AA MQ fraction. Similarly, the AA MQ fraction contained phenylalanine, lysine and tyrosine, which were absent in the AA EDTA fraction. Besides the different monomeric composition of the extracted EPS fractions, the $^{13}$C label distribution in the monomers also varied seasonally (pie charts in Fig. 3a–d).

Up to 23 ± 4 % of the total fixed carbon in the carbohydrate pool was exuded as EPS MQ and up to 6 ± 1 % as EPS EDTA. Similarly, most of the total fixed carbon in the amino acid pool was exuded as EPS MQ rather than as EPS EDTA (46 ± 25 % and 7 ± 2 %, respectively). The percentage of carbon that was initially fixed as carbohydrate and amino acid and subsequently exuded as EPS was in general lowest in June (on average 3 ± 2 %) (dashed line in Fig. 3a–d).

The $^{13}$C label incorporated into the EPS during the first 4 h of the experiment disappeared to a large extent over the course of the experiment (Fig. 3e–h). This was particularly the case for CHO MQ, in which only 20 ± 9 % of the $^{13}$C label remained after 3 d (Fig. 3e). For CHO EDTA and AA MQ, the decrease of $^{13}$C label after 3 d was less (59 ± 21 % and 75 ± 32 % of the incorporated $^{13}$C label remained, respectively). In the case of AA EDTA, 39.3 ± 19.2 % remained after 3 d, except in December when a substantial net label increase was found (Fig. 3h). An increase in the proportioning of deoxy-sugars (fucose and rhamnose) was found in EPS MQ and EPS EDTA while glucose decreased (Fig. 3e,f). Similarly, a shift in the distribution of amino acids was observed.

The loss of $^{13}$C label from the different EPS fractions showed differences among seasons. In the case of the CHO MQ and AA MQ fractions, more label remained 3 d after the application of the label in April and June compared to other months (dashed line in Fig. 3e,g). In the case of the CHO EDTA fraction, less $^{13}$C label remained 3 d after the start of the experiment in February and April, whereas less $^{13}$C label remained in the AA EDTA fraction in February and August compared to other months.

The SCOA in the pore water was composed of formate, acetate, oxalate, malate, lactate, and succinate. Lactate and succinate could not be separated sufficiently well using our LC protocol and are therefore reported as the sum of both. Considerable seasonal changes in the $^{13}$C labeling of succinate + lactate, formate and acetate were observed. Other SCOA were below the limit of detection; hence, only succinate+ lactate, formate, and acetate are depicted in Fig. 4. The concentrations of succinate+lactate (range 2.7 to 5.7 µM), formate (range 3.7 to 13.6 µM), and acetate (range 1.0 to 5.8 µM) in the pore water were high. Labeling of succinate + lactate, formate, and acetate were highest in February and gradually decreased during the year. The percentage of $^{13}$C label that remained in all SCOA 3 d after the start of the experiment increased during the year and ranged from 5 % in February to 42 % in December.

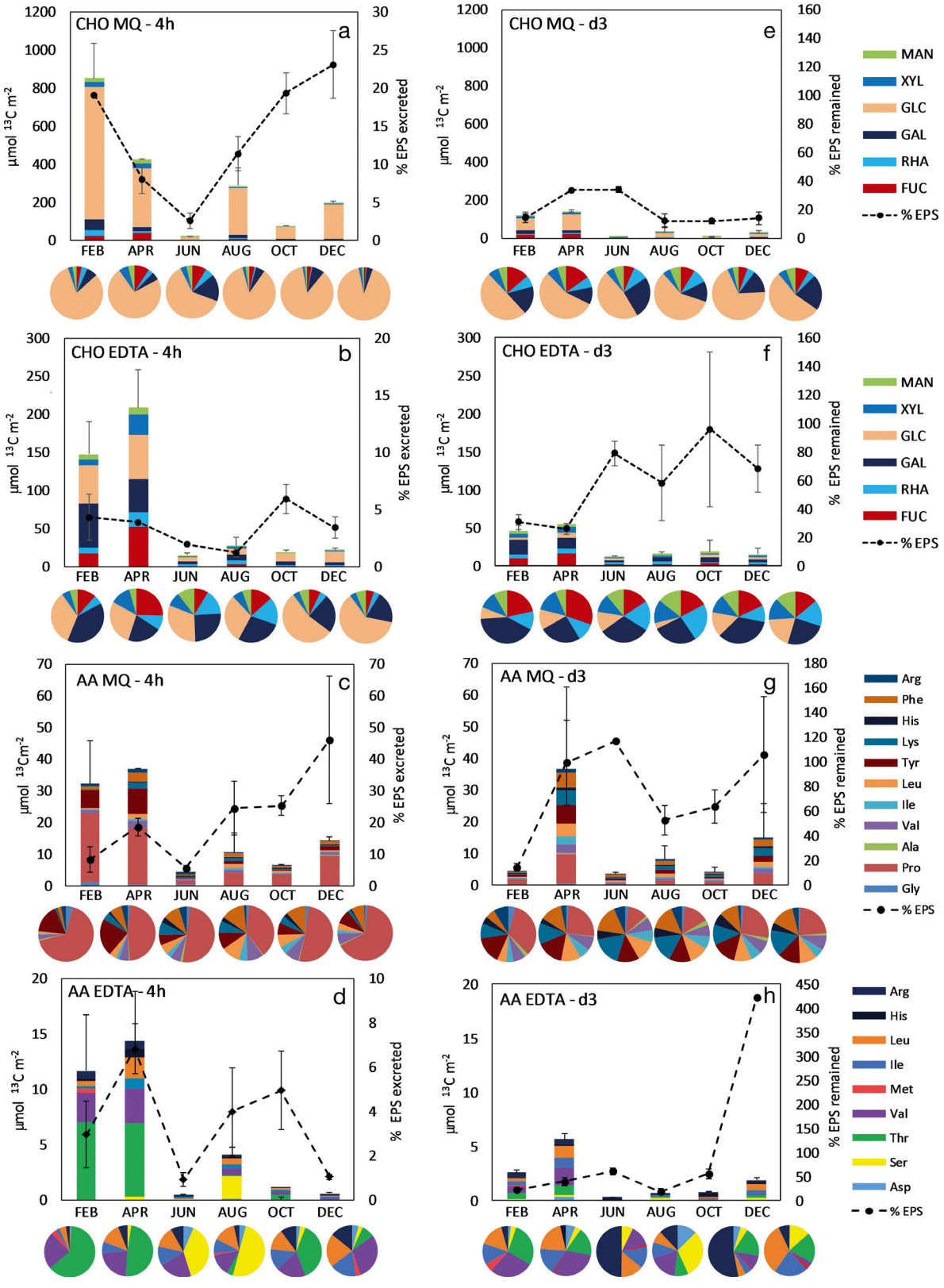


Fig. 3. Annual carbohydrate monomers and amino acids $^{13}C$ label content of water-extractable extracellular polymeric substances (EPS MQ) and EDTA-extractable EPS (EPS EDTA) fractions. Details of $^{13}C$ label are presented for 4 h (i.e. after initial $^{13}C$ label incorporation) and Day 3 (i.e. $^{13}C$ label distribution after 3 d), respectively. In (a–d), the dashed line represents the percentage of carbon initially fixed as carbohydrate and amino acid, respectively, and excreted as EPS. For (e–h), the dashed line represents the percentage of $^{13}C$ label that remained in EPS after 3 d compared to the amount of $^{13}C$ label incorporated at $t = 4$ h. Error bars are ± SD. See Table 2 for further abbreviations

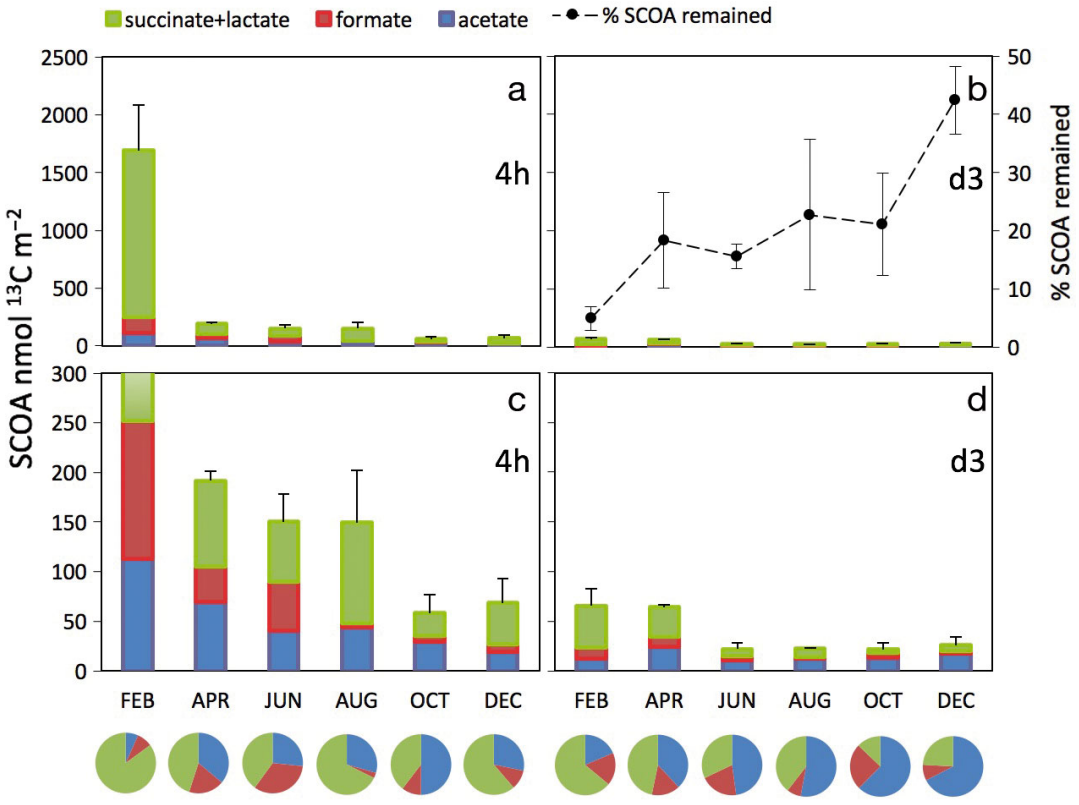


Fig. 4. Annual short-chain organic acid (SCOA) details, for (a,c) 4 h (i.e. after initial $^{13}$C label incorporation) and (b,d) Day 3 (i.e. $^{13}$C label distribution after 3 d). Dashed line in (b) represents the percentage of $^{13}$C label remaining in extracellular polymeric substance (EPS) after 3 d compared to the amount of $^{13}$C label incorporated at $t$ = 4 h. (c) and (d) represent enlargements of (a) and (b), respectively. Error bars are ± SD

### Explanatory variables

Nutrient concentrations in the pore water were always higher than in the water column above the sediment (during immersion) (Table S1 in the Supplement). Inorganic nitrogen was predominantly present as ammonium in the pore water and as nitrate in the overlying water. Average concentrations of pore water inorganic nitrogen were lower in summer (June and August) compared to the rest of the year (27.9 ± 0.1 and 72 ± 27 µmol l$^{-1}$, respectively). N:P ratios above the Redfield ratio (i.e. 16) were observed from February until June (26 ± 5). In August and October, N:P ratios were below the Redfield ratio (7 ± 1), and in December near the Redfield ratio (17 ± 1) (Table S1). Likewise, the concentration of inorganic nitrogen in the overlying water was lower in summer (June and August) compared to the rest of the year (14 ± 3 and 38 ± 16 µmol l$^{-1}$, respectively). The seasonal trend of nutrient N:P ratios in the overlying water was similar to those in the pore water, and ratios were above the Redfield ratio from February until June and in December (46 ± 30) and below the Redfield ratio in August and October (12 ± 2) (Table S1). The pigment fingerprints were typical for diatoms, including β-carotene, chlorophyll *a*, chlorophyll *c*, fucoxanthin, diadinoxanthin and diatoxanthin (Table S1). The photosynthetic parameters $E_k$ and ETR$_{max}$ were higher in spring and summer, while α was higher in autumn and winter (Table S1). PAR correlated to the sediment temperature and was higher in summer than in winter. The average temperature and integrated photon irradiance during the 4 h of $^{13}$C labeling of the diatom mat were lowest in February (3.7°C and 1314 µmol photons m$^{-2}$ and highest in August (20.5°C and 7492 µmol photons m$^{-2}$) (Table S1).

### Production and fate of EPS in relation to explanatory variables

Concordance analysis was done using the dataset for the incorporation rate of $^{13}$C label in monomeric carbohydrates and monomeric amino acids in the EPS extracts (i.e. CHO MQ, CHO EDTA, AA MQ and

AA EDTA) (see Table S2) and explanatory variables (Table S1). The RV-coefficients between the explanatory variables and 3 EPS fractions were significant ($p < 0.05$; CHO MQ was not significant) (Table 1). Results from the concordance analysis are depicted in Fig. 5. The first 2 axes express the major dynamics among the 4 seasonal clusters (i.e. February, April, June/August, and October/December).

The first axis of the concordance analysis of the 3 EPS fractions (i.e. CHO EDTA, AA MQ, and AA EDTA) distinguished autumn and winter (i.e. October, December, and February) from spring and summer (i.e. April, June, and August), whereas the second axis distinguished months during which a high EPS production took place (i.e. February and April) from months with a low EPS production (i.e. June, August, October, and December) (Fig. 5). The nature of the predominant monomeric carbohydrates and amino acids characterized the seasonal clusters (Fig. 5d–f).

Along the first axis of the concordance analysis, the carbohydrates of the EPS (i.e. CHO EDTA fraction) (Fig. 5a) exuded during spring and summer (April, June, and August) showed higher production rates of xylose and rhamnose, and a lower production rate of galactose. In contrast, in autumn and winter (October, December, and February) a high production rate of galactose was observed. Along the second axis, months with a high EPS production (i.e. February and April) showed higher fucose production. The months with low EPS production (i.e. June, August, October, and December) showed high mannose production.

Similar to the carbohydrate component of the EPS, along the first axis of the concordance analysis the AA MQ fraction (Fig. 5b) showed a higher production rate in spring and summer for all amino acids except glycine and proline, which had a lower production rate. Along the first axis, autumn and winter showed a high production rate of glycine and proline and a low production rate of the other measured amino acids. Along the second axis a high production rate of tyrosine and a low production rate of valine were observed. Different than what was seen for the CHO EDTA and AA MQ fractions, the AA EDTA fraction showed a high production rate for most amino acids during June, August, October, and December (i.e. when the production of EPS was low) except for threonine (Fig. 5c). Threonine production rates were high in February and April (i.e. when EPS production was high).

The first axis of the concordance analysis was strongly characterized by temperature and positively associated with PAR, $ETR_{max}$, and $E_k$ (Fig. 5g). Temperature and PAR decreased from June/August to October/December and were associated with an increase in α (i.e. the affinity of photosynthesis for light), β-carotene content, and phosphate- and ammonium concentration in the overlying water. Along the first axis, the increased rates of synthesis of the majority of carbohydrate monomers and amino acids of the CHO EDTA and AA MQ fractions were mainly covariant with light intensity and, to a lesser extent, with sediment temperature, $E_k$, and $ETR_{max}$ (Fig. 5a,b,g). Along the second axis, increased rates of synthesis of amino acids of the AA EDTA fraction were observed. These increased rates of synthesis were consistently associated with a low content of light-harvesting pigments and possibly with insufficient ammonium in the pore water or nitrate in the water column (Fig. 5c,g). Moreover, the high rates of EPS production in February and April were consistently associated with a high content of light harvesting pigments and high concentrations of ammonium in the pore water or nitrate in the water column (Fig. 5g).

By Day 3 after the start of the experiments, the relationship between the proportioning of $^{13}C$ label in the CHO MQ, AA MQ, and AA EDTA fractions (Table S3) and explanatory variables (Table S1) were significant (Table 1). The pattern resulting from the concordance analysis was expressed along 2 main

Table 1. Correlations in the concordance analyses. RV-coefficients range from 0 to 1 and indicate the correlation between the explanatory table and each extracellular polymeric substance (EPS) table. Correlations between axis scores indicate the congruence per axis between the black dots (explanatory) and arrow tips (EPS fraction) in Figs. 5 & 6. **Bold** values indicate significance at p = 0.05. See Table 2 for abbreviations

| EPS fraction | Explanatory vs. production EPS | | | Explanatory vs. $^{13}C$-labeled Day 3 EPS | | |
|---|---|---|---|---|---|---|
| | RV | Pearson's r 1st axis | Pearson's r 2nd axis | RV | Pearson's r 1st axis | Pearson's r 2nd axis |
| CHO MQ | 0.37 | – | – | **0.43** | **0.71** | **0.63** |
| CHO EDTA | **0.59** | **0.76** | **0.91** | 0.40 | – | – |
| AA MQ | **0.67** | **0.76** | **0.77** | **0.72** | **0.94** | **0.84** |
| AA EDTA | **0.81** | **0.90** | 0.56 | **0.56** | **0.82** | **0.83** |

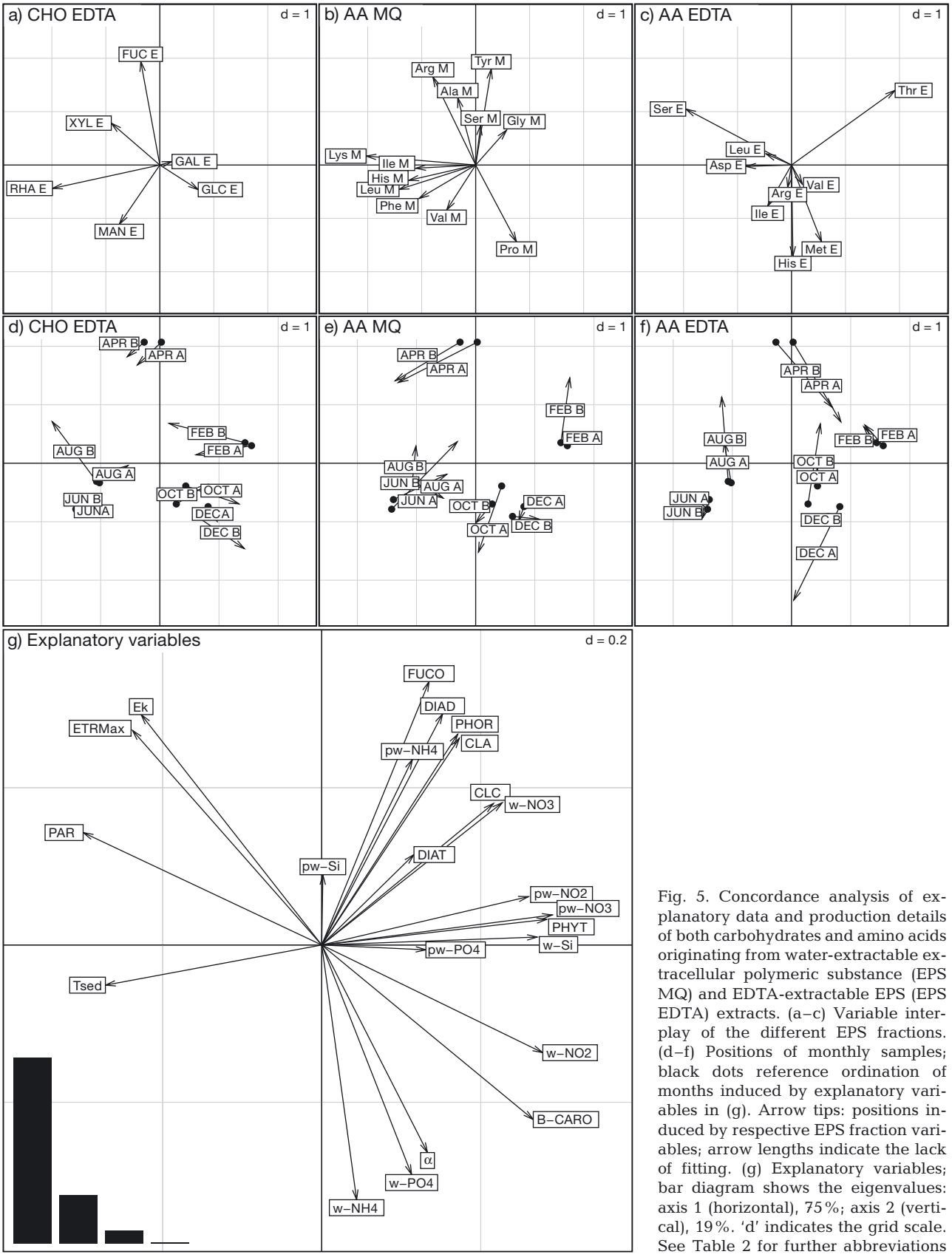


Fig. 5. Concordance analysis of explanatory data and production details of both carbohydrates and amino acids originating from water-extractable extracellular polymeric substance (EPS MQ) and EDTA-extractable EPS (EPS EDTA) extracts. (a–c) Variable interplay of the different EPS fractions. (d–f) Positions of monthly samples; black dots reference ordination of months induced by explanatory variables in (g). Arrow tips: positions induced by respective EPS fraction variables; arrow lengths indicate the lack of fitting. (g) Explanatory variables; bar diagram shows the eigenvalues: axis 1 (horizontal), 75%; axis 2 (vertical), 19%. 'd' indicates the grid scale. See Table 2 for further abbreviations

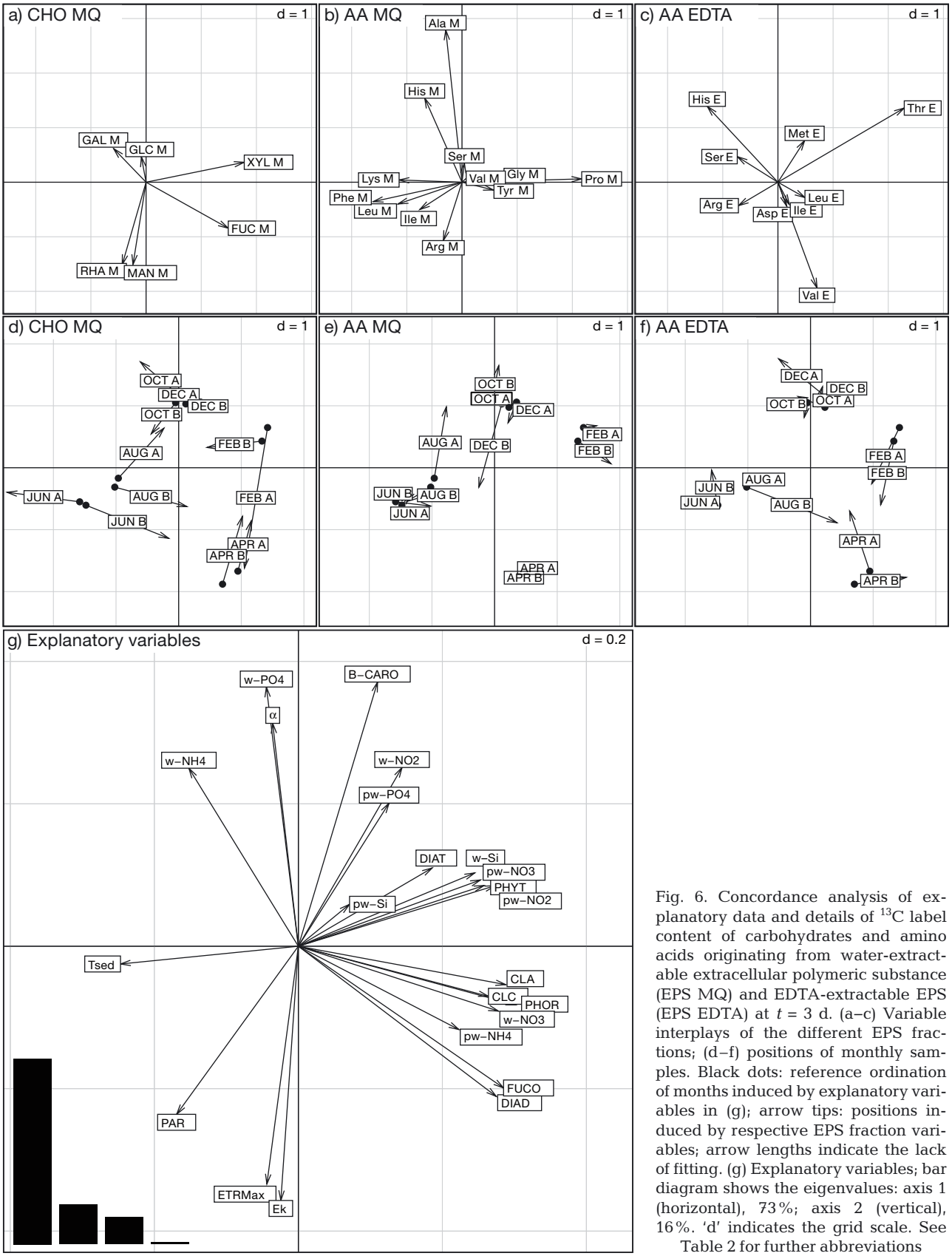


Fig. 6. Concordance analysis of explanatory data and details of $^{13}C$ label content of carbohydrates and amino acids originating from water-extractable extracellular polymeric substance (EPS MQ) and EDTA-extractable EPS (EPS EDTA) at $t$ = 3 d. (a–c) Variable interplays of the different EPS fractions; (d–f) positions of monthly samples. Black dots: reference ordination of months induced by explanatory variables in (g); arrow tips: positions induced by respective EPS fraction variables; arrow lengths indicate the lack of fitting. (g) Explanatory variables; bar diagram shows the eigenvalues: axis 1 (horizontal), 73%; axis 2 (vertical), 16%. 'd' indicates the grid scale. See Table 2 for further abbreviations

axes (Fig. 6g). There was no relationship between the $^{13}C$ label proportioning of the CHO EDTA fraction on Day 3 and the explanatory variables ($p > 0.05$). A seasonal succession similar to the one from the distribution pattern at $t = 4$ h was observed, although the pattern rotated by distinguishing spring and summer (i.e. April, June, and August) from autumn and winter (i.e. October, December, and February) on the second axis (Fig. 6d,e,f). This opposition is seen in the CHO MQ fraction by increases in rhamnose and mannose from autumn and winter to spring and summer, and increases in xylose and fucose from summer and autumn (i.e. June, August, and October) to winter and spring (i.e. December, February, and April) (Fig. 6a,d). For the AA MQ and AA EDTA fractions, the interplay among variables from the $^{13}C$ label distribution pattern at Day 3 (Fig. 6b,c) was similar to the one for the distribution pattern at $t = 4$ h (Fig. 5b,c), except for serine and tyrosine in the AA MQ fraction and leucine, isoleucine, and valine in the AA EDTA fraction (Fig. 6c). At $t = 4$ h, serine and tyrosine in the AA MQ fraction, and leucine, methionine, isoleucine, and valine in the AA EDTA fraction were positioned in, respectively, the June/August and October/December cluster of the concordance plot (Fig. 5b,c). At Day 3, serine and tyrosine did not occur in the AA MQ fraction (Fig. 6b) and leucine, isoleucine, and valine in the AA EDTA fraction were positioned in the February and April clusters (Fig. 6c). This implies that serine and tyrosine (AA MQ fraction), and leucine, isoleucine, and valine (AA EDTA fraction) $^{13}C$ label dynamics were different than for the other amino acids; $^{13}C$ label loss of these amino acids in February and April was low.

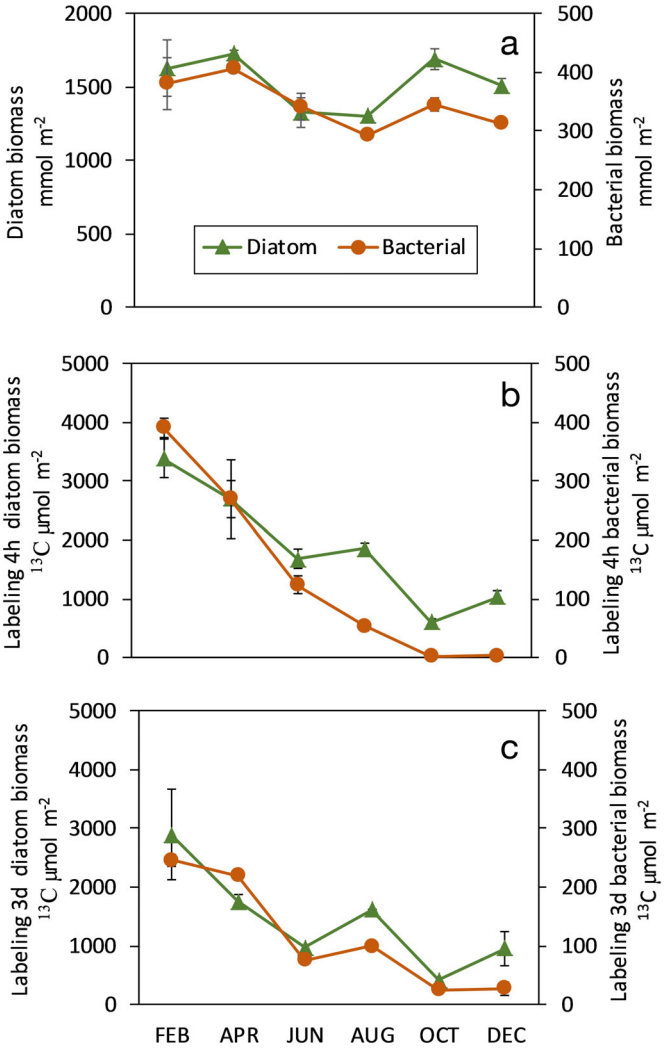


Fig. 7. (a) Annual diatom and bacterial biomass (expressed in mmol C $m^{-2}$), (b) their $^{13}C$ labeling content at 4 h (expressed in µmol $^{13}C$ $m^{-2}$), and (c) their $^{13}C$ labeling content at Day 3 (expressed in in µmol $^{13}C$ $m^{-2}$) calculated from their respective specific phospholipid-derived fatty acids (PLFA)

### Seasonal development of the diatom mat

Benthic diatoms were visible at the sediment surface during the whole year but varied in density, depending on the time of year and time of day. Both the biomass of benthic diatoms and benthic bacteria as estimated from fatty acid biomarker data were lower during summer (June and August) (Fig. 7a). The decrease in biomass coincided with the activity of bioturbating fauna that grazed and disturbed the diatom mat. The annual ratio of diatom to bacterial biomass was constant at ~4.6 (Fig. 7a). The production rate of diatoms and bacteria decreased during the year and was lowest in October and December (Fig. 7b). During February, April, and June, the biomass of diatoms and bacteria seemed to be coupled, as seemed to be the case for the productivity of both groups of organisms. From August onwards, the coupling of the growth of diatoms and bacteria deteriorated and had almost disappeared in December (Fig. 7b). This pattern was retained until Day 3 of the experiment (Fig. 7c). On average, only 1.7 ± 0.9 % of the initially applied $^{13}C$-DIC remained 12 h after the start of the experiment, confirming that most of it was washed out (or exchanged with the atmosphere). In addition, dark fixation of $^{13}C$ label, as was determined in separate sediment core experiments, indicated that $CO_2$ fixation by chemoautotrophic bacteria or through anaplerotic carbon fixation by heterotrophs was not detected in PLFA in dark-incubated (4 h) cores (see 'Material and methods') (results not

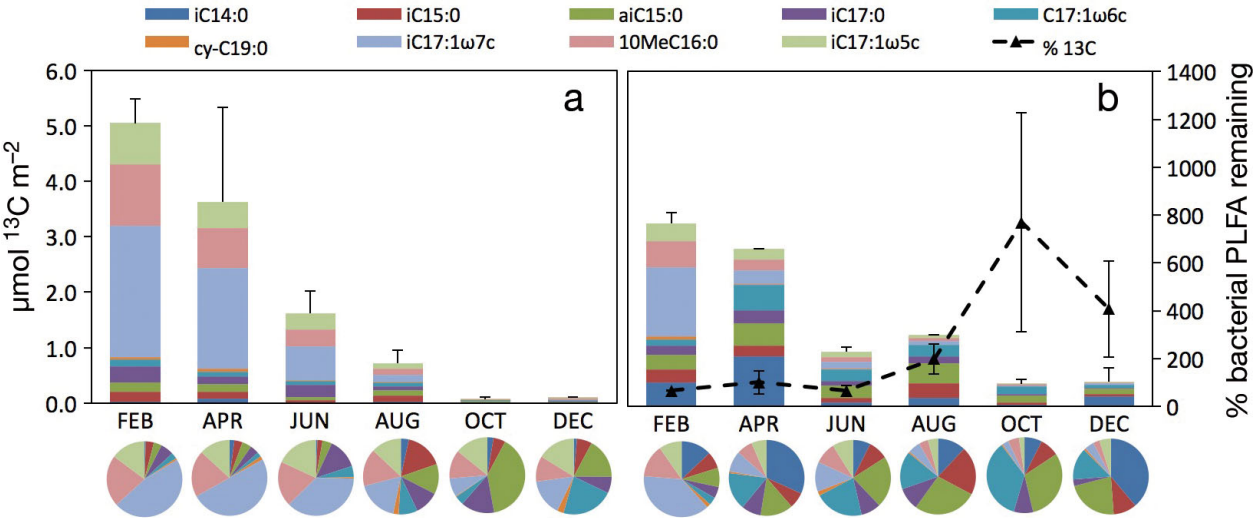


Fig. 8. Annual distribution of $^{13}C$ label in bacterial phospholipid-derived fatty acid (PLFA) biomarkers. Details of $^{13}C$ label are presented for (a) 4 h (i.e. after initial $^{13}C$ incorporation) and (b) after 3 d of $^{13}C$ label distribution. The dashed line in (b) represents the percentage of $^{13}C$ label remaining in bacterial-specific PLFA after 3 d compared to the amount of $^{13}C$ label incorporated at $t = 4$ h

shown), which is in agreement with the conclusions drawn by Miyatake et al. (2014). Hence, the $^{13}C$ label incorporation in heterotrophic bacteria in this study was mainly due to the transfer of organic matter between diatoms and bacteria.

### Production and fate of PLFA bacterial biomarkers

The $^{13}C$ label incorporation in bacterial biomarkers was high at the beginning of the year and gradually decreased towards the end of the year (Fig. 8a). In the first half of the year (i.e. February, April, and June) $^{13}C$ incorporation was dominated by the iC17:ω7c, 10MeC16:0, and iC17:1ω5c biomarkers, whereas in the second half of the year (i.e. August, October, and December) other PLFA biomarkers took over (pie charts in Fig. 8a).

During the year the $^{13}C$ incorporated in the bacterial biomarkers iC17:ω7c, 10MeC16:0, and iC17:1ω5c decreased after 3 d (Fig. 8). This was in contrast to other PLFA, which increased their label content (Fig. 8). During February, April, and June, on average 77 ± 15% of the initially incorporated $^{13}C$ label remained after 3 d (dashed line in Fig. 8b). This was in contrast to the months August, October, and December, when a net gain of label $^{13}C$ was observed. On average, 459 ± 207% of label was gained compared to the amount of incorporated $^{13}C$ label at $t = 4$ h (dashed line in Fig. 8b).

## DISCUSSION

### Production and fate of carbohydrates and amino acids of diatom EPS

The composition of the EPS produced by benthic diatoms is complex, and degradation of this material by microorganisms is a largely unexplored process. The exuded EPS consists mainly of carbohydrates, but amino acids are a component that is consistently present. This type of EPS is common for diatom-dominated biofilms (Granum et al. 2002). Bacterial biofilm assemblages are dominated by proteins rather than by polymeric carbohydrates (Flemming et al. 2000). We found that the composition of the extracted fractions of EPS (EPS MQ and EPS EDTA) differed with respect to carbohydrates and amino acids. This suggests that the synthesis of these 2 operationally defined EPS extracts is under different metabolic control. The carbohydrate composition of EPS MQ was rich in glucose and was produced at a higher rate than the other fractions, suggesting a direct relationship with photosynthesis (de Brouwer & Stal 2001). Glucose can be directly incorporated from chrysolaminaran, while other carbohydrates need to be synthesized first from glucose and therefore would take longer to produce (Underwood & Paterson 2003). Exudates with high glucose content are usually a source of easy degradable carbon for microorganisms. In contrast to EPS MQ, EPS EDTA was rich in deoxysug-

ars (e.g. fucose and rhamnose) and pentoses (e.g. xylose). Deoxysugars and pentoses contribute to the adhesive properties of EPS (Underwood & Paterson 2003) and are more refractory towards degradation (Giroldo et al. 2003).

Although amino acids are a minor component of the EPS in benthic diatom mats, they are important for the structure and properties of these polymers. Lectins (i.e. carbohydrate-binding proteins) link the polysaccharide chains in EPS and thereby contribute to the tertiary structure. This is essential for the biofilm structure, adhesion, and stability (Dugdale et al. 2006). For example, it has been suggested that EPS-proline and EPS-glycine cause adhesion between organisms in soils and give elasticity to the EPS matrix (Redmile-Gordon et al. 2015). The amino acid proline is known to be multifunctional, and its enhanced synthesis could be an important factor in stress acclimation (e.g. salt- and oxidative stress) and serve as an osmo-protectant in certain microorganisms (Van Bergeijk et al. 2003, Szabados & Savoure 2010). Extracellular proline may also serve as an anti-freeze, allowing the presence of liquid water at low temperatures (Wiencke 2011). We conceive that similar functions can be attributed to proline and glycine in diatom mats, particularly because the synthesis of proline and glycine is enhanced in autumn and winter. EPS with a high content of proline and glycine could serve as anti-freeze, and increase elasticity of the EPS matrix of the diatom mat. In this study, we also observed that threonine (in the AA EDTA fraction) was a distinctive and characteristic amino acid because of its high synthesis rate in February and April; i.e. when EPS was produced at high rates. Threonine is known to be associated with algal defense (Buhmann et al. 2016) and therefore might play a role in controlling bacterial activity during the period of high EPS productivity in February and April. In addition, extracellular amino acids are part of enzymes, nutritious polymers or serve as signaling molecules that play a role in diatom cell adhesion and defense processes (Buhmann et al. 2016). Knowledge about the functionality of the substances exuded by diatoms is still limited, but we conceive that the exudation of carbohydrates serves 2 main purposes, namely to allow diatom motility and to maintain their redox balance. At the ecosystem level, these exudations represent an important carbon- and energy source, although due to a lack of nitrogen and other nutrients they are also considered poor food sources for higher trophic levels.

EPS production often changes with the growth phase of the organism, with the level of irradiance or availability of nutrients, or may be linked to endogenous cell rhythms (Underwood & Paterson 2003). The carbon fixed by the benthic diatoms in the present study was exuded rapidly (within 2 h), which agrees with the idea of EPS exudation during photosynthesis as has been suggested by Underwood & Paterson (2003). We observed that a substantial proportion (between 9 and 21%) of the fixed carbon was exuded in the environment as EPS. Other authors reported that this range of fixed carbon released as exudates may be even larger: i.e. between 1.7 and 73%, with a median value between 30 and 40% (Underwood & Paterson 2003).

EPS exudation followed a seasonal pattern, with a lower percentage of fixed carbon exuded in summer compared to the rest of the year, and showed a significant relationship with explanatory variables such as light intensity, temperature, and nutrient concentrations. We conceive that the type of EPS differs depending on the season and that this is related to different functions of EPS, i.e. overflow metabolism or motility. A dense diatom mat rapidly depletes the nutrients from the small volume of pore water. A lack of nutrients during photosynthesis makes balanced synthesis of structural cell material impossible. This results in a situation of unbalanced growth during which the product of photosynthesis is diverted to carbohydrate (overflow metabolism). Eventually, when the intracellular pool of the storage carbohydrate chrysolaminaran is filled up, the excess carbohydrate is exuded as EPS (Stal 2010). Especially in February and April (i.e. high productivity months and a dense diatom mat), the production of EPS should be intimately related to the rate of photosynthesis (de Brouwer & Stal 2001) and EPS exudation should serve as an overflow valve for excess energy (Stal 2010). In June and August, the diatom mat was less dense and EPS production might have been the result of motility, as the diatoms were forced to migrate because of sediment burial due to bioturbation and/or in order to escape high light intensities (Consalvey et al. 2004). During the summer, diatoms are exposed to higher faunal grazing pressure (Pinckney et al. 2003). In October and December, bioturbation and grazing were much lower and overflow metabolism took over again. In addition, EPS produced in summer was more heterogeneous, probably because of the higher synthesis rates of most of the carbohydrate monomers and amino acids. Hence, EPS produced in summer was different in structure compared to the other seasons and their physicochemical properties might therefore have been different. These different physico-

chemical properties could have affected their function and fate in the sediment such as their hydrophobicity and degradability by heterotrophic bacteria (Giroldo et al. 2003). For example, an increase in heterogeneity of EPS in terms of the carbohydrate monomers and amino acids could have led to a more complex structure and a higher recalcitrance to microbial degradation.

The $^{13}C$ label dynamics of CHO MQ indicated a high turnover. The high loss of CHO MQ can be partially explained by washout during tidal inundation, which may account for up to 60% of the EPS loss from the sediment (Underwood & Smith 1998, Hanlon et al. 2006). However, heterotrophic bacteria also consume EPS. This was demonstrated by the enrichment of $^{13}C$ of bacterial-specific PLFA biomarkers coinciding with the loss of CHO MQ, and is consistent with other studies (Goto et al. 2001, Miyatake et al. 2014). EPS EDTA was less influenced by tidal washout and was more refractory against bacterial consumption, which explained its slower turnover. This is consistent with previous studies reporting that deoxy-sugar rich EPS are tightly bound to the sediment and are recalcitrant to bacterial degradation, while hexose-rich polymers are colloidal and more rapidly degraded (de Brouwer & Stal 2001, Giroldo et al. 2003, Hanlon et al. 2006). However, despite these losses, continued isotopic enrichment of EPS indicated new production at the expense of another enriched compound. This enriched compound may be an intracellular carbon source such as chrysolaminaran or an extracellular carbon source such as material derived from degradation of more refractory EPS. Chiovitti et al. (2003) suggested the appearance of a pathway by which EPS EDTA becomes available in the EPS MQ pool by bacterial degradation, for instance, by selective consumption of glucose-rich parts of EPS MQ leaving the more refractory EPS EDTA. Stal (2010) suggested that EPS EDTA might have been derived from initially exuded EPS MQ. This hypothesis is supported by the results of the present study. We observed an increase in the deoxy-sugars of EPS as well as an increase in the isotopic enrichment of EPS EDTA between 12 and 120 h. The transition from one EPS fraction to the other probably also depends on the concentration of divalent cations present in the sediment, such as $Ca^{2+}$ and $Mg^{2+}$, which interact with the EPS (Stal 2010). The binding capacity of these cations enables part of EPS MQ to be eventually transformed into EPS EDTA. In this study, we found seasonal differences of the production and fate of carbohydrate monomers and amino acids in EPS.

### EPS and SCOA as carbon source for bacteria

Heterotrophic bacteria are omnipresent in diatom mats and utilize organic carbon produced by diatoms (Middelburg et al. 2000, Bellinger et al. 2009). Especially early in the year (February, April, and June), the bacterial PLFA biomarkers showed an initial fast uptake of $^{13}C$ label, which was probably the result of the utilization of low-molecular-weight EPS and SCOA exuded by diatoms. Various groups of bacteria used the diatom exudates, as was evidenced by the differences in the level of $^{13}C$ excess values between PLFA biomarkers. The PLFAs i17:1ω7c, i17:1ω5c, and 10Me16:0 are known to be specific for sulfate-reducing bacteria (SRB) (Boschker et al. 1998, Boschker & Middelburg 2002). From February until June the biomass and production of diatoms and bacteria seemed to be coupled. It was concluded that during these months SCOA were the most important substrates for the bacteria. Especially SRB benefited from associating with SCOA-releasing diatoms. From August on, the coupling of biomass and production of diatoms and bacteria weakened, and was almost lost in December. During the period from August until December, EPS produced by diatoms promoted the growth of bacteria other than SRB. The production of SCOA was low from August to December. SRB-utilizing SCOA dominated the community during the first half of the year (i.e. February, April, and June) and showed a higher turnover rate than other bacteria, which dominated the community the second half of the year (i.e. August, October, and December). The seasonal variation of exudates produced by the diatoms played an important role in shaping the community composition and diversity of the associated bacteria.

CHO MQ appeared to be a more important intermediate in the initial transfer of carbon between diatoms and bacteria than CHO EDTA. The amino acids of the EPS were more important in the longer term. After the initial fast transfer of carbon from diatoms to heterotrophic bacteria, a second peak of $^{13}C$ label incorporation in bacteria coincided with, on the one hand, the disappearance of $^{13}C$ label in EPS MQ, and on the other hand, the second release of $^{13}C$ label in EPS MQ and EPS EDTA. It was therefore concluded that this second peak of labeling was due to the ongoing consumption of EPS MQ, as well as the consumption of more recalcitrant EPS (after enzymatic hydrolysis to low-molecular-weight compounds) in the long term (Hunter et al. 2006). Degrading complex EPS is slow; the entire process might take as long as a month (Giroldo et

al. 2003). CHO EDTA seems to be a less favorable carbon source for heterotrophic bacteria (Giroldo et al. 2003).

*Acknowledgements.* We thank Erwin Moerdijk, Wanda Moerdijk, Jelle Moerdijk, Jurian Brasser and Gerjan de Ruiter for assisting in the field sample collection and processing of samples in the laboratory.

## LITERATURE CITED

Admiraal W, Peletier H, Brouwer T (1984) The seasonal succession patterns of diatom species on an intertidal mudflat: an experimental analysis. Oikos 42:30–40

Aitchison J (1983) Principal component analysis of compositional data. Biometrika 70:57–65

Amin SA, Parker MS, Armbrust EV (2012) Interactions between diatoms and bacteria. Microbiol Mol Biol Rev 76:667–684

Bellinger BJ, Underwood GJC, Ziegler SE, Gretz MR (2009) Significance of diatom-derived polymers in carbon flow dynamics within estuarine biofilms determined through isotopic enrichment. Aquat Microb Ecol 55:169–187

Boschker HTS (2004) Linking microbial community structure and functioning: stable isotope ($^{13}C$) labeling in combination with PLFA analysis. In: Kowalchuk GA, de Bruijn FJ, Head IM, Akkermans ADL, van Elsas JD (eds) Molecular microbial ecology, Vol 2. Kluwer Academic Publishers, Dordrecht, p 1673–1688

Boschker HTS, Middelburg JJ (2002) Stable isotopes and biomarkers in microbial ecology. FEMS Microbiol Ecol 40:85–95

Boschker HTS, Nold SC, Wellsbury P, Bos D and others (1998) Direct linking of microbial populations to specific biogeochemical processes by $^{13}C$-labelling of biomarkers. Nature 392:801–805

Boschker HTS, de Brouwer JFC, Cappenberg TE (1999) The contribution of macrophyte-derived organic matter to microbial biomass in salt-marsh sediments: stable carbon isotope analysis of microbial biomarkers. Limnol Oceanogr 44:309–319

Boschker HTS, Moerdijk-Poortvliet TCW, van Breugel P, Houtekamer M, Middelburg JJ (2008) A versatile method for stable carbon isotope analysis of carbohydrates by high-performance liquid chromatography/isotope ratio mass spectrometry. Rapid Commun Mass Spectrom 22:3902–3908

Bruckner CG, Rehm C, Grossart HP, Kroth PG (2011) Growth and release of extracellular organic compounds by benthic diatoms depend on interactions with bacteria. Environ Microbiol 13:1052–1063

Buhmann MT, Schulze B, Förderer A, Schleheck D, Kroth PG (2016) Bacteria may induce the secretion of mucin-like proteins by the diatom *Phaeodactylum tricornutum*. J Phycol 52:463–474

Chessel D, Dufour A, Thioulouse J (2004) The ade4 package. I. One-table methods. R News 4:5–10

Chiovitti A, Bacic A, Burke J, Wetherbee R (2003) Heterogeneous xylose-rich glycans are associated with extracellular glycoproteins from the biofouling diatom *Craspedostauros australis* (Bacillariophyceae). Eur J Phycol 38:351–360

Consalvey M, Paterson DM, Underwood GJC (2004) The ups and downs of life in a benthic biofilm: migration of benthic diatoms. Diatom Res 19:181–202

Cowie GL, Hedges JI (1984) Determination of neutral sugars in plankton, sediments, and wood by capillary gas chromatography of equilibrated isomeric mixtures. Anal Chem 56:497–504

de Brouwer JFC, Stal LJ (2001) Short-term dynamics in microphytobenthos distribution and associated extracellular carbohydrates in surface sediments of an intertidal mudflat. Mar Ecol Prog Ser 218:33–44

Dijkman NA, Kromkamp JC (2006) Phospholipid-derived fatty acids as chemotaxonomic markers for phytoplankton: application for inferring phytoplankton composition. Mar Ecol Prog Ser 324:113–125

Dolédec S, Chessel D (1994) Co-inertia analysis: an alternative method for studying species-environment relationships. Freshw Biol 31:277–294

Dray S, Chessel D, Thioulouse J (2003) Co-inertia analysis and the linking of ecological data tables. Ecology 84: 3078–3089

Dugdale TM, Willis A, Wetherbee R (2006) Adhesive modular proteins occur in the extracellular mucilage of the motile, pennate diatom *Phaeodactylum tricornutum*. Biophys J 90:L58–L60

Edgar LA, Pickett-Heaps JD (1984) Diatom locomotion. Prog Phycol Res 3:47–88

Eilers P, Peeters J (1988) A model for the relationship between light intensity and the rate of photosynthesis in phytoplankton. Ecol Modell 42:199–215

Evrard V, Cook PLM, Veuger B, Huettel M, Middelburg JJ (2008) Tracing carbon and nitrogen incorporation and pathways in the microbial community of a photic subtidal sand. Aquat Microb Ecol 53:257–269

Flemming HC, Wingender J (2010) The biofilm matrix. Nat Rev Microbiol 8:623–633

Flemming HC, Wingender J, Mayer C, Körstgens V, Borchard W (2000) Cohesiveness in biofilm matrix polymers. In: Allison DG, Gilbert P, Lappin-Scott HM, Wilson M (eds) Community structure and cooperation in biofilms. Cambridge University Press, Cambridge, p 87–106

Giroldo D, Vieira AAH, Paulsen BS (2003) Relative increase of deoxy sugars during microbial degradation of an extracellular polysaccharide released by a tropical freshwater *Thalassiosira* sp. (Bacillariophyceae). J Phycol 39: 1109–1115

Goto N, Mitamura O, Terai H (2001) Biodegradation of photosynthetically produced extracellular organic carbon from intertidal benthic algae. J Exp Mar Biol Ecol 257:73–86

Granum E, Kirkvold S, Myklestad SM (2002) Cellular and extracellular production of carbohydrates and amino acids by the marine diatom *Skeletonema costatum*: diel variations and effects of N depletion. Mar Ecol Prog Ser 242:83–94

Hanlon ARM, Bellinger B, Hayes K, Xiao G and others (2006) Dynamics of extracellular polymeric substance (EPS) production and loss in an estuarine, diatom-dominated, microalgal biofilm over a tidal emersion-immersion period. Limnol Oceanogr 51:79–93

Heinzelmann SM, Bale NJ, Hopmans EC, Sinninghe Damsté JS, Schouten S, van der Meer MT (2014) Critical assessment of glyco-and phospholipid separation by using silica chromatography. Appl Environ Microbiol 80: 360–365

Heo M, Gabriel KR (1998) A permutation test of association between configurations by means of the RV coefficient. Commun Stat Simul Comput 27:843–856

Hoagland KD, Rosowski JR, Gretz MR, Roemer SC (1993) Diatom extracellular polymeric substances: function, fine structure, chemistry, and physiology. J Phycol 29:537–566

Hunter EM, Mills HJ, Kostka JE (2006) Microbial community diversity associated with carbon and nitrogen cycling in permeable shelf sediments. Appl Environ Microbiol 72:5689–5701

Kromkamp JC, Forster RM (2003) The use of variable fluorescence measurements in aquatic ecosystems: differences between multiple and single turnover measuring protocols and suggested terminology. Eur J Phycol 38:103–112

Krumböck M, Conrad R (1991) Metabolism of position-labelled glucose in anoxic methanogenic paddy soil and lake sediment. FEMS Microbiol Ecol 8:247–256

Lafosse R, Hanafi M (1997) Concordance d'un tableau avec *K* tableaux: définition de *K* + 1 uples synthétiques. Rev Stat Appl 45:111–126

MacIntyre HL, Cullen JJ (1996) Primary production by suspended and benthic microalgae in a turbid estuary: timescales of variability in San Antonio Bay, Texas. Mar Ecol Prog Ser 145:245–268

McCullagh JSO, Juchelka D, Hedges REM (2006) Analysis of amino acid $^{13}C$ abundance from human and faunal bone collagen using liquid chromatography/isotope ratio mass spectrometry. Rapid Commun Mass Spectrom 20: 2761–2768

McKew BA, Dumbrell AJ, Taylor JD, McGenity TJ, Underwood GJC (2013) Differences between aerobic and anaerobic degradation of microphytobenthic biofilm-derived organic matter within intertidal sediments. FEMS Microbiol Ecol 84:495–509

Middelburg JJ, Barranguet C, Boschker HTS, Herman PMJ, Moens T, Heip CHR (2000) The fate of intertidal microphytobenthos carbon: an in situ $^{13}C$-labeling study. Limnol Oceanogr 45:1224–1234

Miyajima T, Yamada Y, Hanba YT, Yoshii K, Koitabashi T, Wada E (1995) Determining the stable isotope ratio of total dissolved inorganic carbon in lake water by GC/C/IRMS. Limnol Oceanogr 40:994–1000

Miyatake T, Moerdijk-Poortvliet TCW, Stal LJ, Boschker HTS (2014) Tracing carbon flow from microphytobenthos to major bacterial groups in an intertidal marine sediment by using an in situ $^{13}C$ pulse-chase method. Limnol Oceanogr 59:1275–1287

Moerdijk-Poortvliet TCW, Stal LJ, Boschker HTS (2014) LC/IRMS analysis: a powerful technique to trace carbon flow in microphytobenthic communities in intertidal sediments. J Sea Res 92:19–25

Moerdijk-Poortvliet TCW, Van Breugel P, Sabbe K, Beauchard O, Stal LJ, Boschker HTS (2018) Seasonal changes in the biochemical fate of carbon fixed by benthic diatoms in intertidal sediments. Limnol Oceanogr 63: 550–569

Oakes JM, Eyre BD, Middelburg JJ, Boschker HTS (2010) Composition, production, and loss of carbohydrates in subtropical shallow subtidal sandy sediments: rapid processing and long-term retention revealed by $^{13}C$-labeling. Limnol Oceanogr 55:2126–2138

Pierre G, Zhao JM, Orvain F, Dupuy C, Klein GL, Graber M, Maugard T (2014) Seasonal dynamics of extracellular polymeric substances (EPS) in surface sediments of a diatom-dominated intertidal mudflat (Marennes–Oléron, France). J Sea Res 92:26–35

Pinckney JL, Carman KR, Lumsden SE, Hymel SN (2003) Microalgal-meiofaunal trophic relationships in muddy intertidal estuarine sediments. Aquat Microb Ecol 31: 99–108

R Core Team (2015) R: a language and environment for statistical computing. R Foundation for Statistical Computing, Vienna

Redmile-Gordon MA, Evershed RP, Hirsch PR, White RP, Goulding KWT (2015) Soil organic matter and the extracellular microbial matrix show contrasting responses to C and N availability. Soil Biol Biochem 88:257–267

Robert P, Escoufier Y (1976) A unifying tool for linear multivariate statistical methods: the RV-coefficient. Appl Stat 25:257–265

Serôdio J, Vieira S, Cruz S, Barroso F (2005) Short-term variability in the photosynthetic activity of microphytobenthos as detected by measuring rapid light curves using variable fluorescence. Mar Biol 146:903–914

Smith DJ, Underwood GJC (1998) Exopolymer production by intertidal epipelic diatoms. Limnol Oceanogr 43: 1578–1591

Stal LJ (2010) Microphytobenthos as a biogeomorphological force in intertidal sediment stabilization. Ecol Eng 36: 236–245

Szabados L, Savoure A (2010) Proline: a multifunctional amino acid. Trends Plant Sci 15:89–97

Taylor JD, McKew BA, Kuhl A, McGenity TJ, Underwood GJC (2013) Microphytobenthic extracellular polymeric substances (EPS) in intertidal sediments fuel both generalist and specialist EPS-degrading bacteria. Limnol Oceanogr 58:1463–1480

Thioulouse J, Chessel D, Dole S, Olivier JM (1997) ADE-4: a multivariate analysis and graphical display software. Stat Comput 7:75–83

Underwood GJC, Kromkamp J (1999) Primary production by phytoplankton and microphytobenthos in estuaries. Adv Ecol Res 29:93–153

Underwood GJC, Paterson DM (2003) The importance of extracellular carbohydrate production by marine epipelic diatoms. Adv Bot Res 40:183–240

Underwood GJC, Smith DJ (1998) Predicting epipelic diatom exopolymer concentrations in intertidal sediments from sediment chlorophyll *a*. Microb Ecol 35:116–125

Van Bergeijk SA, Van der Zee C, Stal LJ (2003) Uptake and excretion of dimethylsulphoniopropionate is driven by salinity changes in the marine benthic diatom *Cylindrotheca closterium*. Eur J Phycol 38:341–349

Veuger B, Middelburg JJ, Boschker HTS, Houtekamer M (2005) Analysis of $^{15}N$ incorporation into D-alanine: a new method for tracing nitrogen uptake by bacteria. Limnol Oceanogr Methods 3:230–240

Wiencke C (2011) Biology of polar benthic algae. Walter de Gruyter, Berlin

Yallop ML, De Winder B, Paterson DM, Stal LJ (1994) Comparative structure, primary production and biogenic stabilization of cohesive and non-cohesive marine sediments inhabited by microphytobenthos. Estuar Coast Shelf Sci 39:565–582

**Appendix.**

Table A1. Explanatory variables and extracellular polymeric substance (EPS) parameter notation

| Explanatory variables | | EPS parameters | | | |
|---|---|---|---|---|---|
| PAR | Photosynthetically active radiation (400–700 nm) during labeling | Extracellular Polymeric Substances (EPS) | | Amino acids | |
| | | EPS MQ | Water-extractable EPS | Asp | Aspartine |
| $T_{sed}$ | Sediment temperature | EPS EDTA | EDTA-extractable EPS | Ser | Serine |
| Photosynthetic parameters | | Operationally defined EPS fractions | | Thr | Threonine |
| $ETR_{max}$ | Relative maximum reached electron transport rate | CHO MQ | Water-extractable carbohydrates | Gly | Glycine |
| | | CHO EDTA | EDTA-extractable carbohydrates | Pro | Proline |
| α | Light affinity coefficient in the light limited region of the rapid light curve | AA MQ | Water-extractable amino acids | Ala | Alanine |
| | | AA EDTA | EDTA-extractable amino acids | Val | Valine |
| $E_k$ | (minimum) Light saturation irradiance | M | Water-extractable | Met | Methionine |
| Pigments | | Ile | Isoleucine | Leu | Leucine |
| β-CARO | β-Carotene | E | EDTA-extractable | Tyr | Tyrosine |
| CLA | Chlorophyll *a* | Carbohydrates (CHO) | | Lys | Lysine |
| CLC | Chlorophyll *c* | FUC | fucose | His | Histine |
| DIAD | Diadinoxanthine | RHA | rhamnose | Phe | Phenylalanine |
| DIAT | Diatoxanthine | GAL | galactose | Arg | Arginine |
| PHOR | Pheophorbide | GLC | glucose | | |
| FUCO | Pheophorbide | XYL | xylose | | |
| Nutrients | | MAN | mannose | | |
| w-NH4 | Water column ammonium | | | | |
| w-NO2 | Water column nitrite | | | | |
| w-NO3 | Water column nitrate | | | | |
| w-PO4 | Water column phosphate | | | | |
| w-Si | Water column silicate | | | | |
| pw-NH4 | Pore water ammonium | | | | |
| pw-NO2 | Pore water nitrite | | | | |
| pw-NO3 | Pore water nitrate | | | | |
| pw-PO4 | Pore water phosphate | | | | |
| pw-Si | Pore water silicate | | | | |

*Editorial responsibility: Toshi Nagata, Kashiwanoha, Japan*

*Submitted: July 30, 2017; Accepted: January 11, 2018*
*Proofs received from author(s): March 5, 2018*